

Band alignment of heterojunctions formed by $PtSe_2$ with doped GaN

Zhuoyang Lv(吕卓阳), Guijuan Zhao(赵桂娟), Wanting Wei(魏婉婷), Xiurui Lv(吕秀睿), and Guipeng Liu(刘贵鹏)

Citation: Chin. Phys. B, 2025, 34 (**4**): 047304. DOI: 10.1088/1674-1056/adb67b
Journal homepage: http://cpb.iphy.ac.cn; http://iopscience.iop.org/cpb

What follows is a list of articles you may be interested in

Resistive switching behavior and mechanism of HfO_x films with large on/off ratio by structure design

Xianglin Huang(黄香林), Ying Wang(王英), Huixiang Huang(黄慧香), Li Duan(段理), and Tingting Guo(郭婷婷)
Chin. Phys. B, 2024, 33 (**1**): 017303. DOI: 10.1088/1674-1056/ad053a

Modulated optical and ferroelectric properties in a lateral structured ferroelectric/semiconductor van der Waals heterojunction

Shanshan Chen(陈珊珊), Xinhao Zhang(张新昊), Guangcan Wang(王广灿), Shuo Chen(陈朔), Heqi Ma(马和奇), Tianyu Sun(孙天瑜), Baoyuan Man(满宝元), and Cheng Yang(杨诚)
Chin. Phys. B, 2023, 32 (**12**): 127301. DOI: 10.1088/1674-1056/acc7fa

Improved device performance of recessed-gate AlGaN/GaN HEMTs by using *in-situ* N_2O radical treatment

Xinchuang Zhang(张新创), Mei Wu(武玫), Bin Hou(侯斌), Xuerui Niu(牛雪锐), Hao Lu(芦浩), Fuchun Jia(贾富春), Meng Zhang(张濛), Jiale Du(杜佳乐), Ling Yang(杨凌), Xiaohua Ma(马晓华), and Yue Hao(郝跃)
Chin. Phys. B, 2022, 31 (**5**): 057301. DOI: 10.1088/1674-1056/ac48fb

High-performance self-powered photodetector based on organic/inorganic hybrid van der Waals heterojunction of rubrene/silicon

Yancai Xu(徐彦彩), Rong Zhou(周荣), Qin Yin(尹钦), Jiao Li(李娇), Guoxiang Si(侣国翔), and Hongbin Zhang(张洪宾)
Chin. Phys. B, 2021, 30 (**7**): 077304. DOI: 10.1088/1674-1056/abf345

Intrinsic charge transport behaviors in graphene-black phosphorus van der Waals heterojunction devices

Guo-Cai Wang(王国才), Liang-Mei Wu(吴良妹), Jia-Hao Yan(严佳浩), Zhang Zhou(周璋), Rui-Song Ma(马瑞松), Hai-Fang Yang(杨海方), Jun-Jie Li(李俊杰), Chang-Zhi Gu(顾长志), Li-Hong Bao(鲍丽宏), Shi-Xuan Du(杜世萱), Hong-Jun Gao(高鸿钧)
Chin. Phys. B, 2018, 27 (**7**): 077303. DOI: 10.1088/1674-1056/27/7/077303

Band alignment of heterojunctions formed by $PtSe_2$ with doped GaN

Zhuoyang Lv(吕卓阳), Guijuan Zhao(赵桂娟)†, Wanting Wei(魏婉婷), Xiurui Lv(吕秀睿), and Guipeng Liu(刘贵鹏)

School of Physical Science and Technology, Lanzhou University, Lanzhou 730000, *China*

(Received 29 October 2024; revised manuscript received 20 December 2024; accepted manuscript online 15 February 2025)

In order to investigate the effect of different doping types on the band alignment of heterojunctions, we prepared $PtSe_2$/n-GaN, $PtSe_2$/p-GaN, and $PtSe_2$/u-GaN heterojunctions by wet transfer technique. The valence band offsets (VBO) of the three heterojunctions were measured by x-ray photoelectron spectroscopy (XPS), while the $PtSe_2$/n-GaN is 3.70±0.15 eV, $PtSe_2$/p-GaN is 0.264±0.15 eV, and $PtSe_2$/u-GaN is 3.02±0.15 eV. The conduction band offset (CBO) of the three heterojunctions was calculated from the material bandgap and VBO, while the $PtSe_2$/n-GaN is 0.61±0.15 eV, $PtSe_2$/p-GaN is 2.83±0.15 eV, and $PtSe_2$/u-GaN is 0.07±0.15 eV. This signifies that both $PtSe_2$/u-GaN and $PtSe_2$/p-GaN exhibit type-I band alignment, but the $PtSe_2$/n-GaN heterojunction has type-III band alignment. This signifies that the band engineering of $PtSe_2$/GaN heterojunction can be achieved by manipulating the concentration and type of doping, which is significantly relevant for the advancement of related devices through the realization of band alignment and the modulation of the material properties of the $PtSe_2$/GaN heterojunction.

Keywords: van der Waals heterojunction, x-ray photoelectron spectroscopy, band alignment, gallium nitride, platinum diselenide

PACS: 73.22.–f, 68.35.–p, 73.21.–b, 71.20.Nr, 71.20.Be

DOI: 10.1088/1674-1056/adb67b **CSTR:** 32038.14.CPB.adb67b

1. Introduction

In recent years, two-dimensional (2D) materials have shown significant potential for electrical and optoelectronic applications. Due to their distinctive physical and chemical properties, together with their exceptional mechanical strength and flexibility.[1] The capacity to effortlessly generate very thin layers and surfaces with dangling connections in 2D materials is deemed essential for the further progression of Moore's law, particularly regarding more Moore.[2,3] This attribute facilitates the formation of van der Waals heterojunctions (vdWHs) using the simple method of stacking 2D materials. Because van der Waals forces are present rather than covalent bonds, lattice mismatch need not be considered in the context of vdWHs. This significantly lowers the intricacy of synthesis while broadening the spectrum of accessible materials. VdWHs have been used in several electrical and optoelectronic devices owing to their exceptional electronic and photonic features.[4–8]

Gallium nitride (GaN), as a traditional wide-bandwidth semiconductor, has exceptional physical features. These characteristics include a bandgap of 3.4 eV, elevated electron mobility, superior thermal conductivity, and exceptional stability. In comparison to other traditional semiconductors, GaN-based devices exhibit superior efficiency and are appropriate for high-frequency applications. Furthermore, the wide bandgap enables GaN devices to function throughout a broader frequency spectrum and voltage range. These characteristics render GaN extensively used in optoelectronics, leading to the successful development of several high-performance GaN-based optoelectronic devices, including ultraviolet micro-LEDs,[9] self-powered photodiodes,[10] and GaN metalens.[11]

Transition metal dichalcogenides (TMDs) are extensively studied 2D materials. Transition metal dichalcogenides (TMDs) are compounds characterized by the chemical formula MX_2, where M denotes a transition metal (e.g., Mo or W) and X signifies a chalcogen (e.g., S or Se). These compounds possess a multilayer structure and are interconnected by van der Waals forces.[12] TMDs offer numerous advantages compared to other 2D materials, such as enhanced chemical stability, mechanical flexibility, high strength, controllable bandgap, efficient light absorption, and more. These qualities make TMDs highly suitable for a wide range of applications in optoelectronics and energy conversion.[13,14] MoS_2 is now the most extensively researched TMD, used in various devices such as transistors,[15] phototransistors,[16] photodetectors with spectrum response,[17] hydrogen sensors,[18] and other applications. Nevertheless, because to the poor carrier mobility of MoS_2,[19] the absorbance experiences a substantial drop as the thickness increases.[20] Additionally, the manufacturing method is intricate.[21] Consequently, the genuine industrial production of the device is severely restricted. $PtSe_2$, an emerging TMD, surpasses MoS_2 in terms of carrier mobility and long-term air stability.[22] The transition from a semi-

†Corresponding author. E-mail: zhaogj@lzu.edu.cn

© 2025 Chinese Physical Society and IOP Publishing Ltd. All rights, including for text and data mining, AI training, and similar technologies, are reserved.

conductor to a semimetal state can be achieved by decreasing the number of layers in $PtSe_2$. This enables the development of electronic devices with diverse functionalities and enhances its sensitivity to near-infrared light, resulting in a wide range of spectral responses for optoelectronic devices.[23,24] $PtSe_2$ may be produced using several methods and at low temperatures, facilitating large-scale manufacturing. $PtSe_2$ is an exceptionally efficient material for gas sensors and field effect transistors, and it also serves as a basis for the industrial fabrication of these devices.[25,26] The advancement of commercial synthesis methods for $PtSe_2$ necessitates the examination of its heterostructure. GaN serves as an optimal heterostructure substrate for sensitive $PtSe_2$, owing to its broad bandgap, which facilitates the shifting of the absorption edges of the $PtSe_2$/GaN heterojunction into the deep UV region. This results in an augmented migration distance and a decreased carrier complexation rate. Simultaneously, GaN has remarkable environmental stability, enabling the device to function well over a broader spectrum of conditions.[27]

Undoped GaN demonstrates n-type conductivity, which changes during doping. Furthermore, GaN exhibits significant sensitivity to doping, with the particular kind and concentration of dopant profoundly affecting metrics like as mobility, dislocation density, and carrier concentration. Various forms of conductive GaN used as the $PtSe_2$ substrate result in distinct band orientations in the heterojunction. The device's application and performance are governed by the regulation of the impurity type and concentration of the band alignment.[28] Hence, in order to advance the progress of $PtSe_2$/GaN devices, it is essential to assess the impact of different doping types of GaN substrates on the band alignment of the $PtSe_2$/GaN heterojunction.

We fabricated three kinds of heterojunctions using a triple-layer $PtSe_2$ film in conjunction with Si-doped n-type GaN (n-GaN), Mg-doped p-type GaN (p-GaN), and undoped GaN (u-GaN). Utilizing x-ray photoelectron spectroscopy (XPS), we measured the valence band maximum (VBM) and core level (CL) of three heterojunctions. Furthermore, we assessed the band alignment configurations of these heterojunctions using the Kraut formula. This formula may be used to several interfaces, including the insulator-semiconductor interface[29,30] and the organic–inorganic semiconductor interface.[31] It effectively eradicates the surface photovoltage effect of GaN. The band structure may be precisely determined.[32,33] The thickness of $PtSe_2$ was assessed using atomic force microscopy (AFM). We investigate the influence of GaN conductivity type on $PtSe_2$/GaN heterojunctions and the band alignment of heterojunctions created by $PtSe_2$ and GaN with differing conductivities. This study seeks to provide insights for the advancement and fabrication of $PtSe_2$ devices.

2. Experimental details

To evaluate the band alignment of vdWHs, seven samples were prepared: $PtSe_2$/u-GaN heterojunction film, $PtSe_2$/n-GaN heterojunction film, $PtSe_2$/p-GaN heterojunction film, triple-layer $PtSe_2$ film, u-GaN film, n-GaN film, and p-GaN film. The triple layer $PtSe_2$, u-GaN, n-GaN, and p-GaN films used in the experiments were obtained from 6 Carbon Technology (Shenzhen) Co. All three GaN films were prepared by metal–organic chemical vapor deposition (MOCVD) technique using sapphire as the substrate and a low-temperature GaN buffer layer, ammonia (NH_3) as the nitrogen source, and trimethylgallium (TMGa) as the gallium source. n-GaN films were doped with silane (SiH_4) at a concentration of 5×10^{18} cm^{-3}, while p-GaN films were doped with bis-cyclopentadienyl magnesium (CP2Mg) at a concentration of 5×10^{19} cm^{-3}. u-GaN was not doped. All three GaN orientations are (0001). $PtSe_2$ films were fabricated on a copper (Cu) substrate and partially encapsulated with a polymethyl methacrylate (PMMA) layer; the unencapsulated $PtSe_2$ were used as XPS samples. Heterojunctions are fabricated using the wet transfer approach, which is extensively used in heterojunction synthesis, and several studies have shown the efficacy of this method.[34–36] Prior to wet transfer, the GaN surface was ultrasonically cleaned with acetone and ethanol to remove contaminated carbon and oxides from the GaN surface. Furthermore, this process can activate the GaN surface, facilitating the formation of van der Waals forces inside the heterojunction. Figure 1 shows a complete wet transfer process. First, the $PtSe_2$ film was encapsulated in PMMA and three GaN films were cut into squares, with the $PtSe_2$ film slightly smaller than the GaN film. The $PtSe_2$ films were then immersed in 0.1 mol/L freshly prepared ammonium persulfate ($(NH_4)S_2O_8$) solution for 12 hours. After the Cu substrate was completely dissolved, the $PtSe_2$ with PMMA floated to the surface of the solution. The $PtSe_2$ film with PMMA was washed three times in deionized water and then placed on top of the ultrasonically cleaned GaN. The wet film and GaN were tightly adhered to each other by capillary force, and the residual water droplets on the surface of the GaN film were continuously removed by a syringe from one side. $PtSe_2$ was mixed with ultrasonically cleaned GaN film in deionized water, and the residual water droplets on the surface of GaN film were continuously removed with a syringe until the two layers were firmly bonded together. The combined heterojunctions were then dried in a drying oven at 150 °C for 12 hours. This allowed the materials to better bond together. Finally, three heterojunction films were prepared for testing by dissloving the PMMA from the heterojunction surface with acetone.

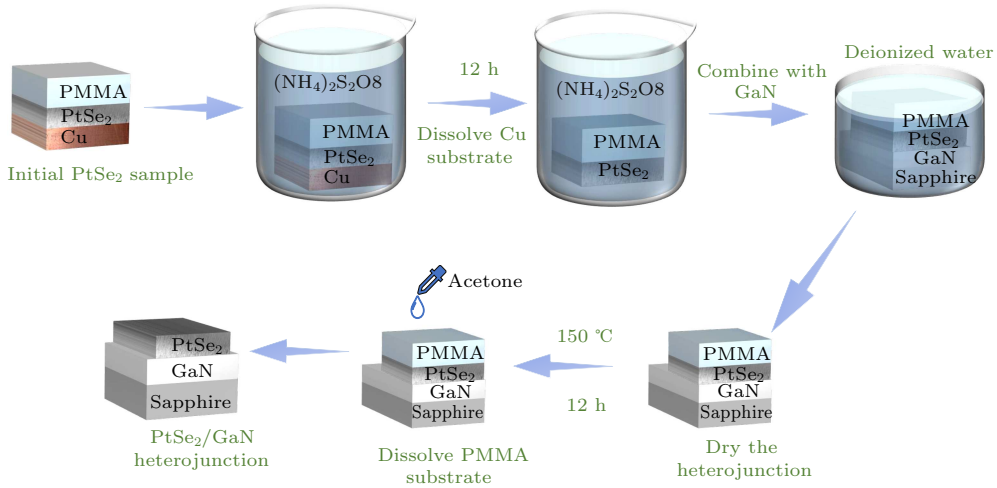


Fig. 1. Diagram of the $PtSe_2$/GaN heterojunction preparation process.

We employed a Kratos Axis Supra XPS measuring apparatus with a monochromatic Al $K\alpha$ ($h\nu = 1486.6$ eV) x-ray radiation source. During XPS of epitaxial GaN, the high-energy electron beam interacts with the sample's surface, causing a rearrangement of the surface charge and resulting in a surface charging effect. The charge effect is often quite pronounced, resulting in a substantial displacement of the measurement findings from the true peak location. To counteract this phenomenon of positive charge, the prevailing approach is to calibrate the XPS spectra by referencing the C 1s peak at 284.8 eV. We have used this calibration procedure consistently across all XPS spectra.The thickness of the $PtSe_2$ coating has been determined measured by AFM (Nanotec Electronica AFM). It should be emphasized that this method of using C 1s as a reference is controversial because of the high uncertainty of C 1s. Considering that the C 1s of the three substrates used in this study are close to each other, this calibration does not affect the conclusions of this study.

3. Results and discussion

3.1. Thickness characterization of $PtSe_2$

We use AFM to characterize the thickness of $PtSe_2$ films. Before AFM testing, standardized calibrations were conducted on the XYZ axes, including drift and noise calibration, displacement measurement error calibration, displacement measurement repeatability calibration, and sub-nanometer height correction scale factor calibration. The calibrated error margin is ± 0.2 nm. The results of our characterization of $PtSe_2$ layers using AFM are shown in Fig. 2, which illustrates the height paraboloid of $PtSe_2$. The observed height difference is 1.57 nm, closely aligning with the thickness of triple-layer $PtSe_2$ reported in the literature.[37] Consequently, we can demonstrate the presence of a triple layer $PtSe_2$ on Cu. The Ga 2p and Pt 4f core levels following heterojunction creation in Fig. 3 remain largely unaltered, indicating the effective synthesis of the heterojunction and the presence of GaN alongside post-transfer $PtSe_2$. Considering the intrinsic corrosion resistance of 2D materials[38] and the stable characteristics of Pt as an inert metal, it is reasonable to anticipate that $PtSe_2$ will exhibit similar properties. Multiple investigations have shown the superior corrosion resistance and stability of $PtSe_2$.[39,40] Thus, it can be inferred that the chemical treatment mentioned above will not cause a major change in the thickness of $PtSe_2$ on the surface of the GaN/$PtSe_2$ heterojunction. In other words, the $PtSe_2$ layer on the GaN surface will continue to have a triple layer structure. Hence, we equate the thickness of $PtSe_2$ on the Cu surface to the thickness of the GaN surface.

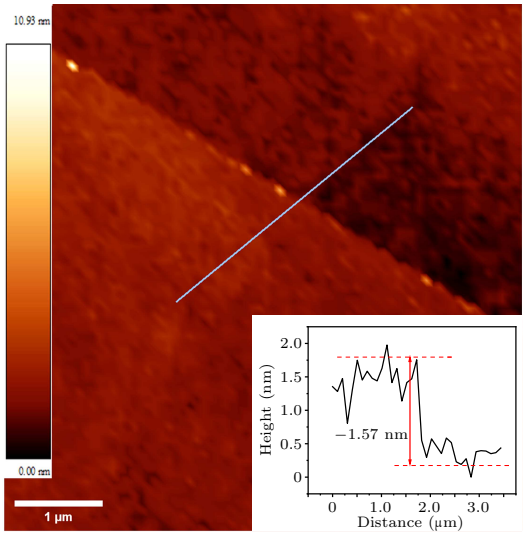


Fig. 2. AFM profile of $PtSe_2$, showing the existence of the triple-layer $PtSe_2$ on Cu.

3.2. Band alignment measured by XPS

The x-ray photoelectron spectroscopy (XPS) has been extensively used in the investigation of heterojunction band alignment, and several studies have verified its high level of accuracy and dependability.[41–43] Once the XPS measures the CL of the relevant element in the sample, the valence band off-

set (VBO or ΔE_V) of the heterojunction may be determined using Eq. (1) established by Kraut *et al.*[44] The conduction band offset (CBO or ΔE_C) of the heterojunction may be determined by considering the bandgap of the material and identifying the band orientation of the heterojunction.

$$\Delta E_V = \left(E_{CL}^{PtSe_2} - E_{VBM}^{PtSe_2}\right) + \left(E_{Ga}^{H} - E_{Pt}^{H}\right) - \left(E_{CL}^{GaN} - E_{VBM}^{GaN}\right), \quad (1)$$

where $(E_{CL}^{PtSe_2} - E_{VBM}^{PtSe_2})$ in Eq. (1) denotes the energy difference between CL of $PtSe_2$ and VBM, $(E_{CL}^{GaN} - E_{VBM}^{GaN})$ denotes the energy difference between the CL of GaN and the VBM, $(E_{Ga}^{H} - E_{Pt}^{H})$ denotes the difference between the CL of GaN and the CL of $PtSe_2$ after the formation of heterojunction. Figure 3 shows the CL and valence band (VB) spectra for all samples. All spectra were obtained using Gaussian–Lorentzian line shape fitting in a Shirley background. The spectra after fitting are very close to the shape of the original XPS measurements. Therefore, it is generally accepted that the deviation of the CL position calculated by fit from the actual position will be within 0.03 eV.[45,46] The VBM is obtained by extrapolating the linear fit from the leading edge of the VBM spectra to the ground state, with an uncertainty of about 0.1 eV.[41] This suggests that the uncertainty in the final VBO and CBO is mainly due to the bias in the VBM.

The Ga 2p CL and VB spectra of n-GaN, p-GaN, and u-GaN films are given in Figs. 3(a), 3(b), and 3(c), respectively. Due to energy splitting caused by spin-orbit coupling, the 2p peak of Ga splits into a pair of symmetrical peaks, which are Ga $2p_{3/2}$ and Ga $2p_{1/2}$. In general, the Ga $2p_{3/2}$ with higher peak intensity was selected as the CL of Ga. The of u-GaN is 2.15 eV, which indicates that the E_F of u-GaN is in the vicinity of the conduction band and the electrons are majority carriers.

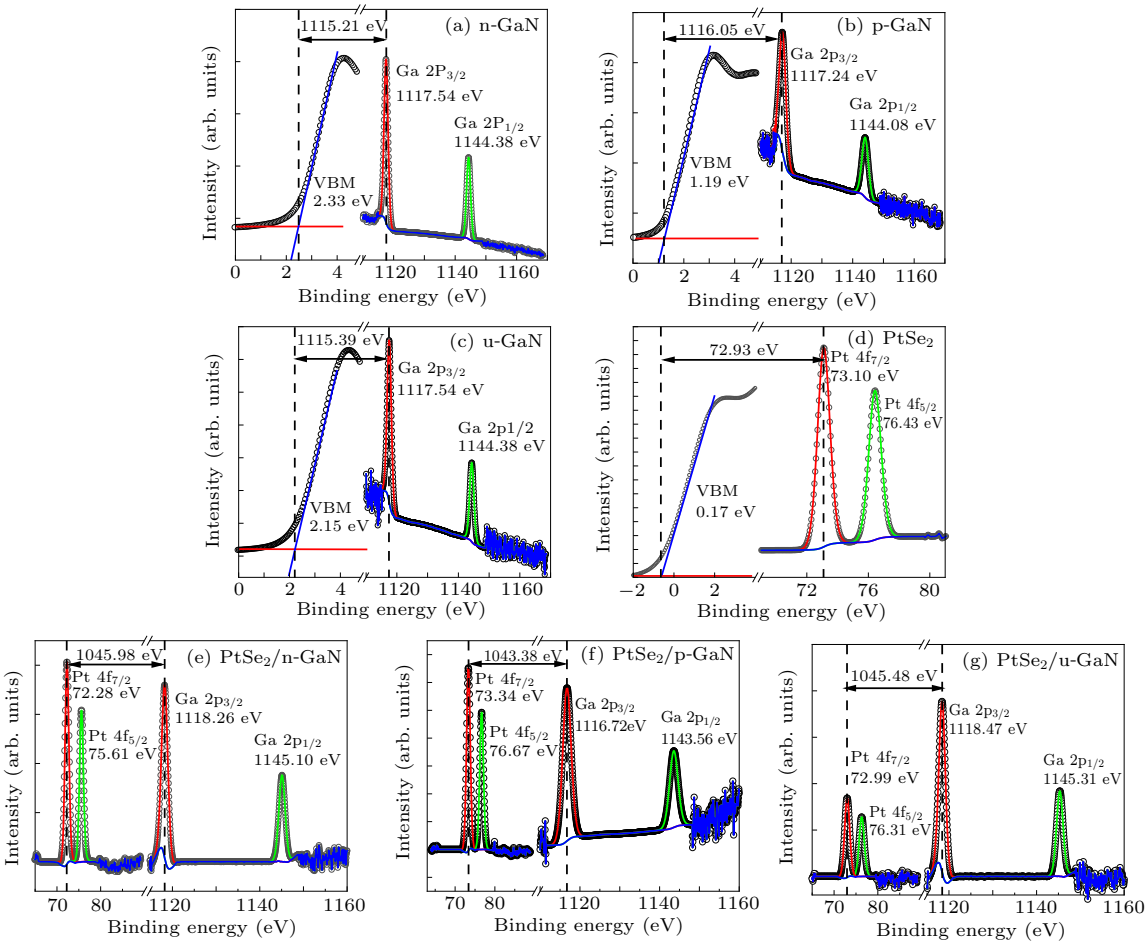
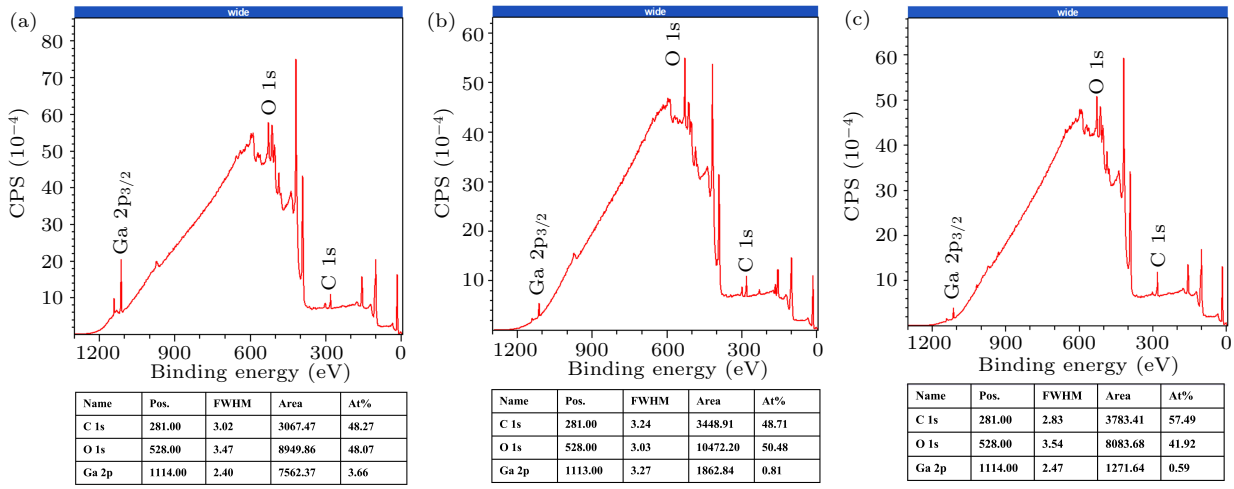


Fig. 3. Ga 2p CL and VB spectra of (a) n-GaN, (b) p-GaN, and (c) u-GaN. (d) Pt 4f CL and VB spectra. Ga 2p and Pt 4f CL spectra of (e) $PtSe_2$/n-GaN heterojunction, (f) $PtSe_2$/p-GaN heterojunction, (g) $PtSe_2$/u-GaN heterojunction.

In contrast to u-GaN, the VBM of p-GaN diminishes considerably to 1.19 eV, whilst the VBM of n-GaN experiences a modest rise to 2.33 eV. This illustrates the impact of doping on the electrical field of semiconductors, which markedly diminishes in acceptor-doped p-GaN and experiences a modest rise in donor-doped n-GaN. This suggests that doping significantly elevates the hole concentration in p-GaN, whilst the electron concentration in n-GaN surpasses that of u-GaN. Given the closeness of the Fermi level in n-GaN and u-GaN, the difference between the core level Ga $2p_{3/2}$ and VBM of both materials is negligible. However, the disparity between the Ga $2p_{3/2}$ and VBM of p-GaN is augmented by about 0.8 eV in

comparison to these two junctions. The reduction in the VBM is attributed to the p-type doping, which produces a downward shift of the Fermi level relative to the other two. This shift is based on the reference of the Fermi level acquired by extrapolation from XPS observations.[47] Nevertheless, the doping has little impact on Ga $2p_{3/2}$, resulting in an amplified disparity between Ga $2p_{3/2}$ and VBM of p-GaN.[48] In Fig. 3(d), a triplelayer $PtSe_2$ sample exhibits only two Pt peaks: Pt $4f_{7/2}$ and Pt $4f_{5/2}$. The Pt $4f_{7/2}$ peak aligns with peaks attributed to the Pt-Se bond in the literature,[49] and the absence of distinguishing Pt–O (72.4 eV) and Pt–Pt (71.0 eV) peaks indicates that the $PtSe_2$ samples are of high purity and have not undergone considerable oxidation. According to the literature, the Pt $4f_{7/2}$ exhibiting the greatest peak intensity was selected as the core stage.[50] Figures 3(e), 3(f), and 3(g) show the CL spectra of Ga 2p and Pt 4f in $PtSe_2$/n-GaN, $PtSe_2$/p-GaN, and $PtSe_2$/u-GaN heterojunctions, respectively. The Pt $4f_{7/2}$ peak (72.99 eV) of $PtSe_2$ before and after heterojunction formation with u-GaN is almost unchanged, but it slightly increases to 73.34 eV and significantly decreases to 72.28 eV after heterojunction formation with p-GaN and n-GaN, respectively. This contrasts with the EF patterns of the three doped GaN types, indicating a potential correlation among them. The CL of the two remaining GaN types diminishes to varying extents after the development of the heterojunction, in contrast to that of u-GaN. The creation of the heterojunction led to a substantial alteration in the CL of the material, indicating the presence of band bending. Furthermore, the core level of $PtSe_2$ on the u-GaN surface demonstrates diminished strength relative to the other two samples. The maximal intensity of the XPS surface measurement technique is significantly affected by the surface area under examination. The wet preparation procedure used fails to completely remove the PMMA, leading to an inconsistency in the quantifiable effective surface area as assessed by XPS. The intensity of $PtSe_2$ at the core level diminishes on the u-GaN surface. Figure 4 shows that the surface states of the three samples are almost the same. Even if the surface differences are taken into account, the surface contamination pattern is not consistent with the above difference pattern, so the above difference is mainly a result of the shift of the Fermi level. Substituting the values in Fig. 3 into Eq. (1), the VBO of the $PtSe_2$/n-GaN, $PtSe_2$/p-GaN, and $PtSe_2$/u-GaN heterojunctions were calculated as 3.70 eV, 0.26 eV, and 3.02 eV, respectively.



Name	Pos.	FWHM	Area	At%
C 1s	281.00	3.02	3067.47	48.27
O 1s	528.00	3.47	8949.86	48.07
Ga 2p	1114.00	2.40	7562.37	3.66

Name	Pos.	FWHM	Area	At%
C 1s	281.00	3.24	3448.91	48.71
O 1s	528.00	3.03	10472.20	50.48
Ga 2p	1113.00	3.27	1862.84	0.81

Name	Pos.	FWHM	Area	At%
C 1s	281.00	2.83	3783.41	57.49
O 1s	528.00	3.54	8083.68	41.92
Ga 2p	1114.00	2.47	1271.64	0.59

Fig. 4. Substrate broad spectra: (a) n-GaN, (b) p-GaN, (c) u-GaN.

To calculate the conduction band offset (CBO or ΔE_C), use Eq. (2) after determining the VBO and sample bandgap.

$$\Delta E_C = E_g^{GaN} - \Delta E_V - E_g^{PtSe_2}. \tag{2}$$

In previous studies, the bandgap of GaN was assumed independently independent of doping for calculating CBO. Three varieties of GaN with the same prohibited bandgap $E_g^{GaN} = 3.40$ eV are used.[51,52] Bandgap of $PtSe_2$ may be related to production and measuring methods.[49,55] It is generally accepted that the bandgap of bulk $PtSe_2$ is 0 eV, monolayer $PtSe_2$ is 1.2 eV, and bilayer $PtSe_2$ is 0.21 eV. The literature indicates that the bandgap of large-area triple-layer $PtSe_2$, synthesized by CVD on a silicon substrate using platinum tetrachloride ($PtCl_4$) and selenium (Se), was measured at 0.31 eV based on absorption spectra.[50] We choose to accept this finding, which implies that $E_g^{PtSe_2} = 0.31$ eV. However, it should be emphasized that the bandgap for different thicknesses of $PtSe_2$ is not definitive and is currently determined by experimental and theoretical calculations. Substituting ΔE_V and $E_g^{PtSe_2}$, E_g^{GaN} into Eq. (2), the CBO of $PtSe_2$/n-GaN, $PtSe_2$/p-GaN, and $PtSe_2$/u-GaN heterojunctions were determined as 0.61 eV, 2.8 eV, 0.07 eV, respectively. Figure 5 shows the band alignment diagrams for the three heterojunctions. The $PtSe_2$/p-GaN and $PtSe_2$/u-GaN heterojunctions feature type-I band alignment. In contrast, the $PtSe_2$/n-GaN heterojunction features a type-III band alignment.

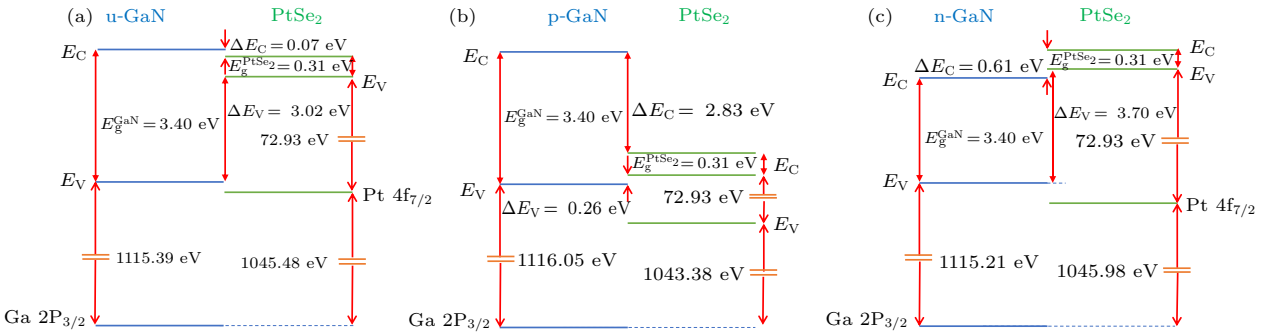


Fig. 5. Band alignment diagrams of (a) $PtSe_2$/u-GaN, (b) $PtSe_2$/p-GaN, (c) $PtSe_2$/n-GaN.

3.3. Heterojunction band offset

Figures 6(a) and 6(b) show the original band of n-GaN, u-GaN, and $PtSe_2$ before heterojunction formation and the band bending after heterojunction formation. The n-GaN and u-GaN have the same type of conductivity, so the band bending of GaN and $PtSe_2$ in the two heterojunctions is in the same direction, where GaN bends down and $PtSe_2$ bends up. The direction of band bending results from the various work functions of the two materials. The work function of $PtSe_2$ is typically measured to be 4.35 eV at a thickness of 1.4 nm, and 4.43 eV at a thickness of 2.2 nm.[53] The work function of the $PtSe_2$ triple layer that we use should fall within a certain range. The typical electron affinity measurement of GaN is 3.5 eV, then the work function of n-GaN is 4.57 eV and that of u-GaN is 4.85 eV, respectively, combined with the XPS measurement.[54] As the work function of the material increases, the energy of the electrons decreases. Consequently, when a heterojunction contact is formed, the electrons will move from the high-energy material to the low-energy material. In other words, they will move from the material with a lower work function to the material with a higher work function. As a consequence, electrons progressively migrate from $PtSe_2$ to the n-GaN and u-GaN surfaces, leading to the accumulation of negative charges on the GaN surface and a downward displacement of the band. The band bending process and outcomes of the MoS_2/GaN heterojunction are identical. However, the degree of bending is different. For the $PtSe_2$/n-GaN heterojunction, the E_C of n-GaN decreases drastically and is lower than that of $PtSe_2$ by 0.61 eV, while for the $PtSe_2$/u-GaN heterojunction, the E_C of u-GaN decreases only slightly and remains higher than that of $PtSe_2$. More precisely, the size of band offset on the surface of $PtSe_2$/n-GaN heterojunction is 1.54 eV (0.93 eV + 0.61 eV), and for $PtSe_2$/u-GaN heterojunction it is only 1.04 eV (1.11 eV − 0.07 eV). The band offset of $PtSe_2$/n-GaN heterojunction is larger, indicating that the built-in potential is larger. This is due to Si is amphiphilic active in GaN and has a low surface density of states and zero density, so high doping leads to saturation of electron concentration in GaN and degradation of the GaN surface, with elevated surface potentials, increasing the degree of band bending.[56–58] On the other hand, the high Si concentration also causes significant tensile stresses on the GaN surface,[59,60] which can narrow the GaN bandgap and have a direct effect on the heterojunction band offset.[61,62] This eventually results in a substantial increase in EF, ultimately indicating a type-III band alignment. We assert that by meticulously regulating the doping concentration of Si, $PtSe_2$/n-GaN may achieve type-II band alignment, consistent with theoretical simulations.[27] Figures 6(c) and 6(d) show the amount of band bending before and after the the $PtSe_2$/p-GaN generation heterojunction compared to the $PtSe_2$/u-GaN heterojunction with the same band alignment. The bending direction of $PtSe_2$/p-GaN heterojunction is opposite to that of $PtSe_2$u-GaN, with p-GaN bending upward and $PtSe_2$ bending downward. Both heterojunctions should exhibit the same direction of band bending when considering the work function. Nevertheless, the experimental findings contradict this notion. This occurrence may be attributed to a mix of many variables, with the Fermi level pinning effect being the primary component we hypothesize. Several studies have confirmed the notable Fermi level pinning effect in Mg-doped p-GaN.[63,64] This effect causes the hole mobility to no longer be determined by the difference in material work function, but rather by the position of the surface Fermi level. The constrained Fermi level causes in the transportation of holes to the surface of p-GaN, leading to the accumulation of holes at the surface and the upward bending of the surface band with positive charge. The clamped Fermi level induces the movement of holes in p-GaN towards the surface, leading to the buildup of holes at the surface and the upward bending of the positively charged surface band. Similarly, the total band offset at the $PtSe_2$/p-GaN heterojunction interface can be calculated to be 0.76 eV (2.83 eV − 2.07 eV). Astonishingly, the band offset of $PtSe_2$/p-GaN heterojunction is lower than that of $PtSe_2$/u-GaN. This indicates that Mg-doped p-GaN with $PtSe_2$ establishes a built-in potential that is significantly diminished relative to its state prior to doping. Magnesium has dual behavior in GaN: it acts as an acceptor when substituting for a gallium atom and as a double donor in the interstitial location. At elevated doping concentrations, the free energy of Mg at the interstitial site decreases, resulting in Mg's propensity to act as a double donor. This behavior lowers the net hole concentration of the material, thus raising the Fermi level and decreasing the surface potential.[63]

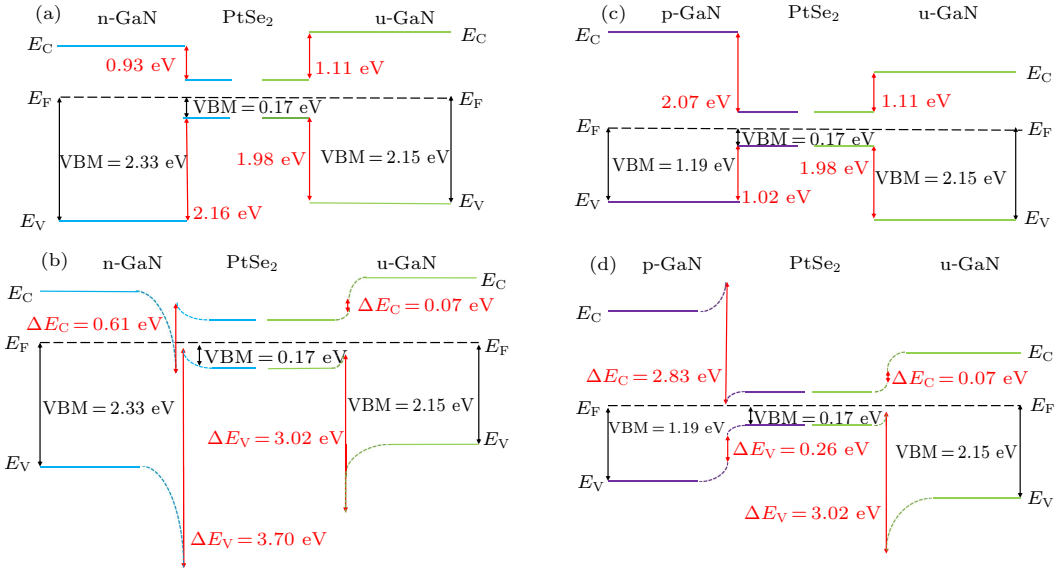


Fig. 6. (a) Initial band diagram of n-GaN, u-GaN, and $PtSe_2$. (b) Schematic band bending of n-GaN, u-GaN, and $PtSe_2$ after heterojunction formation. (c) Initial band diagram of p-GaN, u-GaN, and $PtSe_2$. (d) Schematic diagram of band bending after heterojunction formation of p-GaN, u-GaN, and $PtSe_2$. As a visual reference, the E_F of the material in the image above is aligned.

The C-plane (0001) of GaN is a polar surface exhibiting significant spontaneous polarization effects.[65] This generates a dipole at the junction interface, leading to alterations in the electronic energy levels next to the interface and a modification in band bending. The interfacial dipole phenomenon produces band bending as well as interface states, which affects the device's long-term stability and performance,[65] and additional research into the dipole effect on the heterojunction structure is required.

4. Conclusion

In summary, we have used XPS to investigate the influence of different GaN doping types upon the band alignment of the $PtSe_2$/GaN heterojunction. We found that the $PtSe_2$/u-GaN and $PtSe_2$/p-GaN heterojunctions are both type-I band alignments, with opposite magnitudes of VBO and CBO, but the $PtSe_2$/n-GaN heterojunction is type-III. The high Si doping concentration degrades the GaN surface and increases the surface potential, resulting in a higher band offset than the $PtSe_2$/n-GaN heterojunction. The band offset of the $PtSe_2$/p-GaN heterojunction is smaller than that of the undoped case, which is due to the high concentration of Mg doping, which causes Fermi level pinning, E_F being fixed at a higher position, the net hole concentration decreasing, and the surface potential decreasing. This suggests that the heterojunction band orientation is affected by both the substrate's doping type and concentration. The doping type affects the direction of band bending, whereas the doping concentration affects the substrate surface potential, resulting in a change in band offset. Consequently, for narrow bandgap semiconductors like triple-layer $PtSe_2$, it is essential to consider the doping concentration of the substrate, since even a little alteration in this concentration might result in a shift in the kind of band alignment. This is advantageous for heterojunction band engineering and serves as a reference for the future development of $PtSe_2$/GaN heterojunction devices.

Acknowledgements

Project supported by the National Natural Science Foundation of China (Grant No. 61874108), the Fundamental Research Funds for the Central Universities (Grant No. lzujbky-2024-04), and the Gansu Provincial Scientific and Technologic Planning Program (Grant No. 22ZD6GE016).

References

[1] Karim Khan, Ayesha Khan Tareen, Muhammad Aslam, Wang R H, Zhang Y P, Mahmood Asif, Ouyang Z B, Zhang H and Guo Z Y 2020 *J. Mater. Chem. C* **8** 387
[2] Zeng S, Tang Z, Liu C and Zhou P 2021 *Nano Research* **14** 1752
[3] Fiori G, Bonaccorso F, Iannaccone G, Palacios T, Neumaier D, Seabaugh A, Banerjee S K and Colombo L 2014 *Nat. Nanotechnol.* **9** 768
[4] Xia W, Dai L, Yu P, *et al*. 2017 *Nanoscale* **9** 4324
[5] Yu X, Wang X, Zhou F, Qu J and Song J 2021 *Adv. Funct. Mater.* **31** 2104260
[6] Hu W and Yang Jinlong 2017 *J. Mater. Chem. C* **5** 12289
[7] Chen X, Pan W Guo, Guo R Tang, Hu X, Bi Z Xu and Wang J 2022 *J. Mater. Chem. A* **10** 7604
[8] Li T, She Y, Yan C, Miao J and Jariwala D 2023 *MRS Bull.* **48** 899
[9] Yu H, Memon M H, Wang D, Ren Z, Zhang H, Huang C, Tian M, Sun H and Long S 2021 *Opt. Lett.* **46** 3271
[10] Song W, Chen J, Li Z and Fang X 2021 *Adv Mater.* **33** 2101059
[11] Chen B, Wu P, Su V, *et al*. 2017 *Nano Lett.* **17** 6345
[12] Manzeli S, Ovchinnikov D, Pasquier D, Yazyev O V and Kis A 2017 *Nat. Rev. Mater.* **2** 17033
[13] Upadhyay S N, Satrughna J A K and Pakhira S 2021 *Emergent Mater.* **4** 951
[14] Yin X, Tang C S, Zheng Y, *et al*. 2021 *Chem. Soc. Rev.* **50** 10087
[15] Radisavljevic B, Radenovic A, Brivio J, Giacometti V and Kis A 2011 *Nat. Nanotechnol.* **6** 147
[16] Yin Z, Li H, Li H, *et al*. 2012 *ACS Nano* **6** 74

[17] Xie Y, Zhang B, Wang S, *et al*. 2017 *Adv. Mater.* **29** 1605972
[18] Baek D H and Kim J 2017 *Sensors and Actuators B: Chemical* **250** 686
[19] Yu Z, Ong Z, Li S, *et al*. 2017 *Adv. Funct. Mater.* **27** 1604093
[20] Bernardi M, Palummo M and Grossman J C 2013 *Nano Lett.* **13** 3664
[21] Hu Y, Li X, Lushington A, *et al*. 2013 *ECS J. Solid State Sci. Technol.* **2** 3034
[22] Wang G, Wang Z, McEvoy N, Fan P and Blau W J 2021 *Adv. Mater.* **33** 2004070
[23] Kandemir A, Akbali B, Kahraman Z, *et al*. 2018 *Semicond. Sci. Technol.* **33** 085002
[24] Ghasemi F, Taghavimendi R and Bakhshayeshi A 2020 *Opt. Quantum Electron* **52** 492
[25] Zhao Y, Qiao J, Yu Z, *et al*. 2017 *Adv. Mater.* **29** 1604230
[26] Mc Manus J B, Horvath D V, Browne M P, *et al*. 2020 *Nanotechnology* **31** 375601
[27] Meng X, Shen Y, Liu J, *et al*. 2021 *Applied Catalysis A: General* **624** 118332
[28] Kim K S, Oh C S, Lee W H, *et al*. 2000 *J. Crystal Growth* **210** 505
[29] Fares C, Ren F, Lambers E, *et al*. 2018 *Semicond. Sci. Technol.* **34** 025006
[30] Yan B, Liu S, Heng Y, *et al*. 2017 *Nanoscale Res. Lett.* **12** 363
[31] Lee D, Zhou J, Chen G, *et al*. 2019 *Adv. Electron. Mater.* **5** 1800624
[32] Sezen H, Ozbay E, Aktas O, *et al*. 2011 *Appl. Phys. Lett.* **98** 111901
[33] Lewandków R, Grodzicki M and Mazur P 2021 *Surf. Rev. Lett.* **28** 2150077
[34] Um D, Lee Y, Lim S, Park Seungyoung, Lee Hochan and Ko Hyunhyub 2016 *ACS Appl. Mater. Interfaces* **8** 33955
[35] Kang M S, Lee W Y, Yoon Y G, Choi J W, Kim G S, Kim S H, Park N W and Lee S K 2022 *ACS Appl. Mater. Interfaces* **14** 51881
[36] Fang C Z, Wang Y B, Li T Z, Zeng X Y, Li X X, Yang J Y, Wang D, Zhang H R, Liu Y, Hao Y and Han G Q 2024 *Laser Photon. Rev. Early View* 2401001
[37] Yu X, Yu P, Wu D, *et al*. 2018 *Nat. Commun.* **9** 1545
[38] Mujib S, Santanu Mukherjee, Ren Z, *et al*. 2020 *Royal Soc. Open Sci.* **7** 200214
[39] Zhao Y 2016 "High impermeability and layer-dependent electronic properties of two-dimensional layered materials", PolyU Electronic Theses
[40] Zhou Z, Xu T, Zhang C, *et al*. 2021 *Nano Research* **14** 1704
[41] Hong SK, Hanada T, Makino H, *et al*. 2001 *Appl. Phys. Lett.* **78** 3349
[42] Chiu M H, Tseng W H, Tang H L, *et al*. 2017 *Adv. Funct. Mater.* **27** 1603756
[43] Tamin C, Chaumont D, Heintz O and Adnane M 2020 *Surf. Interface Analysis* **52** 985
[44] Kraut E A, Grant R W, Waldrop J R and Kowalczyk S P 1980 *Phys. Rev. Lett.* **44** 1620
[45] Li H, Liu X, Sang L, *et al*. 2014 *Phys. Status Solidi B* **251** 788
[46] Fan H B, Sun G S, Yang S Y, *et al*. 2008 *Appl. Phys. Lett.* **92** 192107
[47] Wang T, Jing C Q, Dong W H, Zhang J H and Zhang Y 2010 *Mol. Biol. Rep.* **37** 1099
[48] Tangi M, Mishra P, Tseng C, *et al*. 2017 *ACS Appl Mater. Interfaces* **9** 9110
[49] Bhorkar K, Sygellou L, Cathelinaud M, Ren D, Adam J L and Yannopoulos S N 2022 *ACS Appl. Electron. Mater.* **4** 4814
[50] Wang W, Li K, Wang Y, Jiang W, Liu X and Qi H 2019 *Appl. Phys. Lett.* **114** 201601
[51] Su S C, Zhang H Y, Zhao L Z, He M and Ling C C 2014 *J. Phys. D: Appl. Phys.* **47** 215102
[52] Cook T E, Fulton C C, Mecouch W J, *et al*. 2003 *J. Appl. Phys.* **93** 3995
[53] Chung C, Yeh H, Wu P, *et al*. 2021 *ACS Nano* **15** 4627
[54] Wu C I, Kahn A, Taskar N, *et al*. 1998 *J. Appl. Phys.* **83** 4249
[55] Zhang L, Yang T, Sahdan MF, *et al*. 2021 *Adv. Electron. Mater.* **7** 2100559
[56] Köhler K, Wiegert J, Menner H P, Maier M and Kirste L 2008 *Appl. Phys.* **103** 023706
[57] Siol S, Hellmann J C, Tilley S D, *et al*. 2016 *ACS Appl Mater Interfaces* **8** 21824
[58] Halidou I, Benzarti Z, Chine Z, Boufaden T and El Jani B 2001 *Microelectron. J.* **32** 137
[59] Chine Z, Rebey A, Touati H, *et al*. 2006 *Phys. Status Solidi (a)* **203** 1954
[60] Krost A, Dadgar A, Strassburger G and Clos R 2003 *Phys. Status Solidi (a)* **200** 26
[61] Schenk H P D, Borenstain S I, Berezin A, *et al*. 2008 *J. Appl. Phys.* **103** 103502
[62] Xie J, Mita S, Rice A, *et al*. 2011 *Appl. Phys. Lett.* **98** 202101
[63] Miceli G and Pasquarello A 2016 *Phys. Rev. B* **93** 165207
[64] Hashizume T 2003 *J. Appl. Phys.* **94** 431
[65] Idé J, Mothy S, Savoyant A, Alain Fritsch, *et al*. 2013 *Int. J. Quantum Chem.* **113** 580